Ann. Telecommun.
DOI 10.1007/s12243-009-0131-0

Extension of the FDTD Huygens subgridding to frequency dependent media

Fumie Costen · Jean-Pierre Bérenger

Received: 2 December 2008 / Accepted: 17 September 2009

Abstract A wide range of wireless system developments require knowledge of the distribution of electromagnetic fields from various sources in humans. As experimental assessment is ethically unacceptable, high-resolution numerical dosimetry is needed. The finite-difference time-domain method is the most appropriate due to its simplicity and versatility. Reduction in demands on computational resources can be achieved using subgridding techniques. This paper rigorously introduces frequency dependency to one of the most promising subgridding techniques, Huygens subgridding. The validity of the Huygens surface in lossy media, as well as on the physical interface, is intensively studied.

Keywords Huygens surface · Subgrid · Finite-difference time-domain · Debye media · UWB · Numerical method · Numerical dosimetry

1 Introduction

With the rapid and wide spread of the use of the mobile telecommunications, concerns about the adverse health effects of the exposure to signals emitted from devices such as mobile phones have increased. Exposure assessment in humans is ideally performed experimentally. However, the logistics of an experimental assessment become extremely tedious and volunteer studies are normally viewed as ethically unacceptable. Therefore, precise representation of the electromagnetic field distribution in human tissues can be achieved by numerical modelling with realistic heterogeneous models of the human body. Numerical methods have matured for frequent use for dosimetric calculation. Recent work [1, 2] reveals that propagation characteristics depend on the frequency and radio environment of interest and ultra wide band (UWB) signals penetrate deeper and deposit less energy than a continuous wave. Understanding of the UWB propagation characteristics in such a wide range of radio environments can be achieved by the simulation of transient wave propagation.

Unlike such techniques as the method of moments, finite element method, geometrical theory of diffraction or the physical theory of diffraction, the various finite difference time domain (FDTD) methods offer the ability to analyse arbitrarily complex, wideband problems and are simple to implement. Some tissues in the human body have geometrically complicated fine structures, and their high relative permittivity makes the wavelength of interest shorter than that in air. Therefore, in FDTD space, a spatial sampling resolution $9 \sim 15$ times higher than needed for the sampling of free-space is required for numerical modelling of the interior of the human body. This means that computational memory requirements can easily exceed that available, and prohibit rigorous study with adequate accuracy when the physical space of interest and its surroundings are spatially and uniformly sampled at an ideal high resolution.

F. Costen (✉)
School of Electrical and Electronic Engineering,
The University of Manchester, Sackville Street Building,
Manchester, M60 1QD, UK
e-mail: f.costen@cs.man.ac.uk

J.-P. Bérenger
Centre d'Analyse de Défense, 16 bis, Avenue Prieur de la
Côte d'Or, 94114, Arcueil, France
e-mail: jean-pierre.berenger@dga.defense.gouv.fr

Published online: 03 October 2009

To reduce the memory requirement, a variety of subgridding techniques have been proposed [3–7]. Many of these techniques focus on interpolation at the interface, and a computational procedure is simpler than other methods, which require matrix inversion [8–10]. In these techniques, the main grid regions have the same temporal discretisation as that in the subgrid regions, minimising later instability. However, [11] proposes a method to overcome this inefficiency. Nevertheless, the ratio between the coarse and fine meshes in these schemes are usually limited to fivefold variation, to minimise spurious reflections at the interface. When the field distribution in the fine mesh region is not the major concern of the numerical simulation, macromodel [12] is an alternative to subgridding schemes. However, careful interpolation at the interface is the key for a stable calculation, and a matrix inversion is required to produce the transfer function.

The work [13, 14] has proposed a solid method, referred to as Huygens subgridding (HSG), to connect these different mesh regions based on the Huygens–Kirchhoff principle [15]. The advantages of this method are the absence of a restriction on the ratio of spatial resolutions and a lack of significant numerical reflections from the interfaces between the different meshing regions; also, a matrix inversion is not required. To meet the need to simulate the propagation and absorption of electromagnetic energy in biological tissues, this paper extends the HSG–FDTD [13, 14] to frequency-dependent media. Although the extended HSG–FDTD is, in theory, valid in the general three-dimensional (3D) case, in this paper, it is only tested in the 1D case. Two numerical experiments are reported. The first one is a simple test case that validates the principle of the method. The second experiment is more complex, with a computational domain that is composed of several subgrids, with several human tissues. This experiment is representative of the propagation of waves through the torso of a human body and is a first step toward realistic 3D problems. The technical terminology on HSG in this paper is the same as in [13].

2 Huygens surfaces in Debye media

The equivalence theorem states that a field produced within a given part of space by sources located outside this part can be reproduced by impressing the electric current $\boldsymbol{J_s}$ and magnetic current $\boldsymbol{K_s}$ upon the surface separating the two parts

$$\boldsymbol{J_s} = \boldsymbol{n} \times \boldsymbol{H}_i; \quad \boldsymbol{K_s} = -\boldsymbol{n} \times \boldsymbol{E}_i, \tag{1}$$

where $\boldsymbol{n}$ is the unit vector normal to the surface, oriented in the direction opposite to the sources, and $\boldsymbol{E}_i$ and $\boldsymbol{H}_i$ are the electric and magnetic fields that would exist upon the surface if the sources were present. The surface where equivalent currents are set is called a Huygens surface in numerical electromagnetics [16].

The HSG method [13] relies on the use of two Huygens surfaces. The inner surface (IS) radiates the field from a coarse grid called space-A to a fine grid called space-B, and the outer surface (OS) radiates the field from the fine grid to the coarse grid. The HSG method has been described and tested [13, 14] in the case that IS and OS are placed in a vacuum. This paper extends it to the first-order Debye media.

The equivalence theorem is valid for any medium [17]. From this, the Huygens surface can be used to impress an incident wave in any medium, especially in Debye media. As a consequence, the HSG can be extended to Debye media. In the following, we only write down FDTD equations in the 1D case, but the extended HSG is valid in the general 3D case as well. Let us consider a 1D FDTD grid in a Debye medium with the polarisation of the electric flux density D_y and H_z depicted in Fig. 1. The FDTD scheme in this medium [18] involves using the Maxwell equations to advance in time quantities $\boldsymbol{D}$ and $\boldsymbol{H}$, with, in addition, an auxiliary equation to obtain the $\boldsymbol{E}$ field from $\boldsymbol{D}$ at every $\boldsymbol{D}$ node. Assume that the incident wave propagates to the right and that the Huygens surface is placed as depicted in Fig. 1, between the $\boldsymbol{D}$ and $\boldsymbol{H}$ nodes. Consider the Maxwell–Faraday equation

$$\frac{\partial D_y}{\partial t} = \frac{\partial H_z}{\partial x} - \mathcal{J}_y, \tag{2}$$

where $\mathcal{J}_y$ is a current density. In view of discretising Eq. 2 at node $D_y(0)$, $\boldsymbol{J_s}$ can be set equal to the incident field $\boldsymbol{H}_i$ at the physical location of node $H_z(1/2)$, that is $\boldsymbol{J_s} = -H_{i_z}(1/2) \cdot \boldsymbol{i_y}$, where $\boldsymbol{i_y}$ is the unit vector in direction y. With $\mathcal{J}_y(0) = \boldsymbol{J_s}/\Delta x$, where Δx is the spatial sampling, the discretisation of Eq. 2 yields

$$D_y^{n+1}{}_{(0)} = D_{y(0)}^n - \frac{\Delta t}{\Delta x}\left[H_z^{n+\frac{1}{2}}\left(\frac{1}{2}\right) - H_z^{n+\frac{1}{2}}\left(-\frac{1}{2}\right)\right] + \frac{\Delta t}{\Delta x} H_{i_z}^{n+\frac{1}{2}}\left(\frac{1}{2}\right) \tag{3}$$

As in a vacuum [16], this equation can be interpreted as the regular FDTD equation at node $D_{y(0)}$ in the scattered region because the additional term subtracts

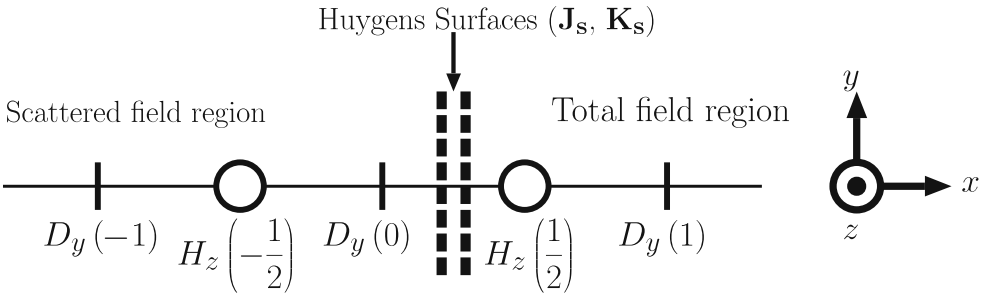

Fig. 1 1D electric flux density and magnetic field

the incident field from the total field. Equation 3 is identical to the corresponding equation in a vacuum, with just $\boldsymbol{D}$ in place of $\epsilon_0 \boldsymbol{E}$, where ϵ_0 is the permittivity in free space. The Maxwell–Ampere equation in a vacuum is left unchanged in the Debye medium, so that its discretised form is also left unchanged at node $H_z(\frac{1}{2})$, that is,

$$H_z^{n+\frac{1}{2}}\left(\frac{1}{2}\right) = H_z^{n-\frac{1}{2}}\left(\frac{1}{2}\right) - \frac{\Delta t}{\mu_0 \Delta x}\left[E_{y(1)}^n - E_{y(0)}^n\right] + \frac{\Delta t}{\mu_0 \Delta x} E_{i_y(0)}^n, \quad (4)$$

where μ_0 is the permeability in free space. As a summary, in a Debye medium, an incident wave can be impressed in an FDTD grid by using the same FDTD equations as in a vacuum at the two nodes located aside the current sheets in Eq. 1, with just $\epsilon_0 \boldsymbol{E}$ replaced with $\boldsymbol{D}$ in the discretised Faraday–Maxwell equation. This permits the HSG method to be generalised in a straightforward manner to Debye media. At both the IS and the OS Huygens surfaces, the same FDTD equations as in [13] are used. Consider, for instance, the IS surface. Equation 3 is used with the incident field H_{i_z} equal to the H_z component in the coarse grid computed as in [13]. For the implementation of Eq. 4, E_{i_y} is computed as in [13] using E_y obtained from D_y by means of the auxiliary equation like at every node of the Debye medium. Filtering procedures used in [13] to remove the late time instability can be introduced as in [13] by using several coarse nodes to compute the filtered incident fields E_{i_y} and H_{i_z}.

3 Numerical verification

Section 3 verifies the HSG scheme in the first-order Debye media in two kinds of situations: the radio environment of Section 3.1 has a single medium whose medium parameters reproduce human fat tissue used in Section 3.2. A set of eight media are modelled in Section 3.2, which demonstrates one of the possible future applications of HSG. A soft source is applied for excitation, and there is no filtering used, unlike [13].

3.1 Validity of HSG in a Debye medium

The stability and accuracy of the production of the Huygens surfaces are examined by placing OS and IS in a homogeneous medium. The relative permittivity ϵ_r of the medium is a function of the angular frequency ω as $\epsilon_r = \epsilon_\infty + (\epsilon_S - \epsilon_\infty)/(1 + \jmath\omega\tau_D) + \sigma/(\jmath\omega\epsilon_0)$, where the optical permittivity ϵ_∞ and the statical permittivity ϵ_S are 3.91 and 6.05, respectively, and the relaxation time τ_D is 26.9 ps and the conductivity σ is $2.98{\cdot}10^{-2}$ S/m.

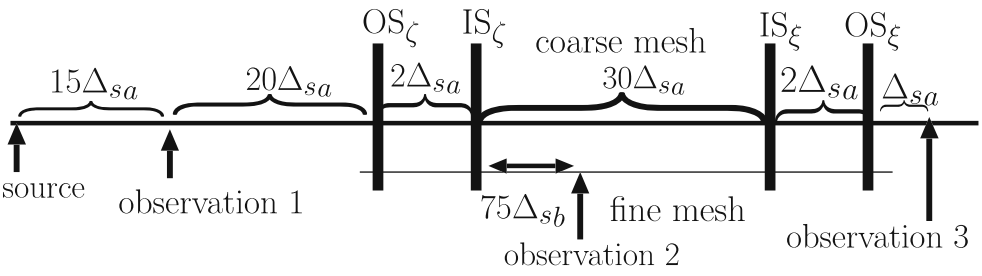

Fig. 2 The location of three observation points relative to the Huygens surfaces IS and OS and source excitation

These four parameters fit the frequency-dependent permittivity and conductivity of human fat measured at the frequency range centred at 6.8 GHz shown in [19]. Figure 2 depicts the geometrical relationship of source excitation and observations and the Huygens surfaces, i.e., IS and OS. The mesh ratio is set to 15. The soft source excitation is placed 37 Δs_a away from IS_ζ in the main grid, where Δs_a is 0.1/30 m. The source excitation is a modulated Gaussian, the same as in [20] with $f_{CW} = 3$ GHz, $w = 0.75$, $\alpha \fallingdotseq 2.267$. Figure 3a is $\boldsymbol{E}$ at the source excitation, normalised in amplitude. The centre frequency is 6.8 GHz. The temporal sampling Δt_a in the coarse mesh is set to $\Delta s_a/(\sqrt{3}\upsilon)$, where υ is the speed of light in the air. The signal propagating from the source is first observed 15 Δs_a away from the source and then observed (37 $\Delta s_a + 75\ \Delta s_b$) away from the source in the subgrid, whose spatial sampling Δs_b is $0.1/(30 \times 15)$ m. The third observation is 70 Δs_a away from the source in the main grid. Since the coarse mesh region is terminated by the perfectly matched layer (PML) boundary condition [21], only the incoming signal from the source should be observed at each observation location. At 6.8 GHz, the relative permittivity of the media is about 4. Therefore, the wave propagates at about half the speed of the light in the medium.

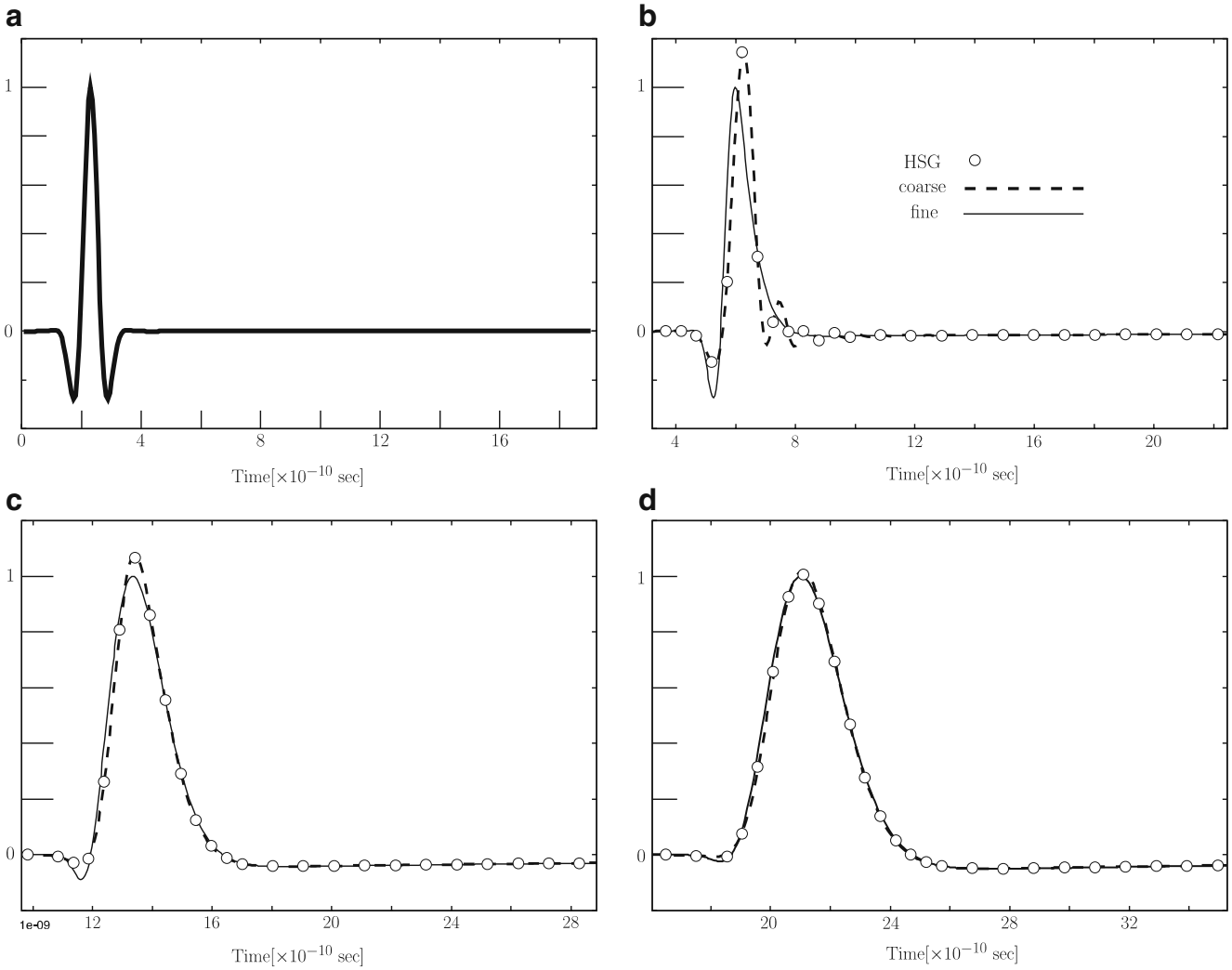

Fig. 3 Three observations depicted in Fig. 2 for verification of the interface between the main grid and subgrid. **a** The waveform at the source excitation. **b** $\boldsymbol{E}$ observed at observation 1 in Fig. 2 in case of (1) FDHSG scheme, (2) standard uniform meshing whose mesh size is the same as the main grid region of FDHSG scheme, and (3) standard uniform meshing whose mesh size is the same as the subgrid region of FDHSG scheme. $\boldsymbol{E}$ at observation 2 and 3 are in **c** and **d**, respectively. Signals are normalised with respect to $\boldsymbol{E}$ observed from the case of 3. **b** The validation of OS_ζ and IS_ζ, **c** and **d** validate IS_ξ and OS_ξ, respectively

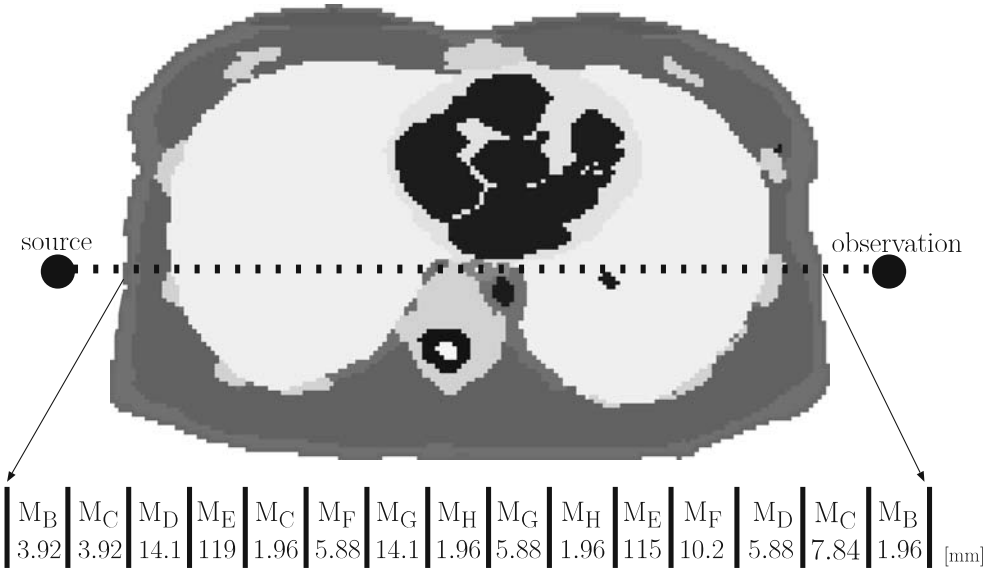

Fig. 4 Cross section of a man 1.342 m from the ground. The MRI data are a 2-mm-resolution model of NORMAN provided by the Radiation Protection Division, Health Protection Agency. It is assumed that the UWB signal propagates through this human body from the left-hand side to the right-hand side. This paper models the tissues on the dotted line in 1D FDTD space. The tissue codes $\mathrm{M}_B \sim \mathrm{M}_H$ under the image correspond to Table 1. The thickness of each tissue is shown in millimetres. Seventy-five percent of the tissues on the *dotted line* are M_E of the lung

This information is used to estimate the time of arrival of the possible signal leaking at the interfaces. If there is a signal leak from OS_ζ to observation 1, the leaking signal will be observed roughly at 1.4 ± 0.2 ns. If there is a signal leak from IS_ξ to observation 2, the leaking signal will be observed roughly at 2.2 ± 0.2 ns. $\boldsymbol{E}$ observed at these three observation locations are plotted as ∘ in Fig. 3b, c and d. As a reference, the entire space is uniformly sampled with $\Delta s_{\mathrm{ref}} = \Delta s_a$ and observed signals are plotted as the thick dotted line. The thin lines in Fig. 3 are obtained with the uniform sampling with $\Delta s_{\mathrm{ref}} = \Delta s_b$. As expected, $\boldsymbol{E}$ from HSG scheme in Fig. 3b is identical to $\boldsymbol{E}$ from the coarsely meshed FDTD because the incident pulse propagates

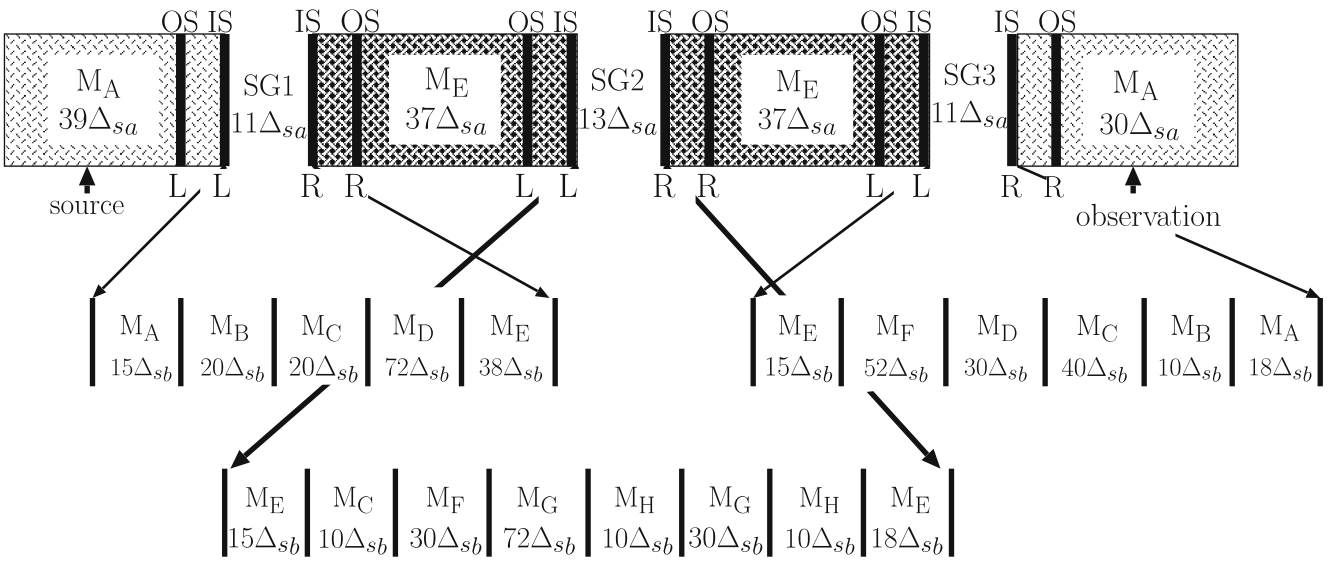

Fig. 5 The radio environment setting with subgridding. The mesh ratio $\Delta s_a / \Delta s_b$ is 15

Table 1 Media parameters in the first-order Debye model

Tissue code	Tissue	σ [S/m]	ϵ_∞	ϵ_S	τ_D [ps]
M_A	Air	0	1	1	0
M_B	Skin	0.49	30	79	62
M_C	Fat	$3{\cdot}10^{-2}$	3.5	6.2	39
M_D	Muscle	0.7	42	100	49
M_E	Lung	0.3	14	36	48
M_F	Bone	$1.9{\cdot}10^{-2}$	4.2	9.5	77
M_G	Oesophagus	1	37	73	25
M_H	Heart muscle	0.58	48	280	206

Gabriel et al. [19] presents the media parameters of these human tissues based on the fourth-order Cole–Cole model. These values are used to obtain the media parameters for the first-order Debye model at the centre frequency of 6.8 GHz

upon the same coarse grid part in the two calculations, and then experiences the same numerical dispersion that filters its highest frequencies. $\boldsymbol{E}$ from HSG scheme in Fig. 3c is comparative to $\boldsymbol{E}$ from the coarsely meshed FDTD. What is important is that neither Fig. 3b nor c shows any spurious signals. These validate OS_ζ and IS_ζ and IS_ξ. $\boldsymbol{E}$ from HSG scheme in Fig. 3d is in between $\boldsymbol{E}$ in FDTD with coarse meshing and $\boldsymbol{E}$ in FDTD with fine meshing. This validates OS_ξ. The calculation, performed with up to 10^5 time steps, was totally stable without filtering.

3.2 Application to human body

The radio environment for 1D frequency-dependent (FD) HSG–FDTD was determined based on magnetic resonance imaging (MRI) data. A cross-section of a human torso is shown in Fig. 4. The tissues on the straight line are modelled in the FDTD space as depicted in Fig. 5. Note that three subgrids are used. It is assumed that the UWB signal is emitted about 59 mm away from the left-hand side of the torso and propagates along the horizontal line in Fig. 4.

The first-order Debye media parameters for each tissue are presented in Table 1. The central frequency to be used is 6.8 GHz, and the corresponding wavelength is sampled by 15 points in every 2.94 mm ($\triangleq \Delta s_a$) in the air.

The skin has a thickness of 2 mm, which is the resolution of the MRI data. The skin can be modelled using $2\Delta s_a/3$ without the media parameters being taken into consideration. In other words, two cells in the fine mesh region can be used to model the skin when the subgridding region has a meshing ratio of 3. In reality, the modelling of the radio environment should be based not only on geometrical, but also on numerical, accuracy. To achieve a reasonable numerical accuracy, the relative permittivity ϵ_r of the tissues has to be taken into account. For the skin, ϵ_r at 6.8 GHz is about 40, and the wavelength at 6.8 GHz in the skin becomes 8 mm. Little numerical dispersion in the skin would be experienced if the wavelength is sampled by 40 points. A mesh ratio of 15 (i.e., $15\Delta s_b = \Delta s_a$) achieves this numerical accuracy.

The signal propagates through skin, fat, and muscle, reaching the lung. During this propagation, the centre frequency has been lowered by 6 GHz. When the signal arrives at the lung, the highest frequency of interest is about 1.4 GHz. Here, the frequency, whose spectrum shows −3 dB relative to the peak spectrum, is called the highest frequency of interest. Thirteen points sample 1.4 GHz in the lung in a grid of space step Δs_a. From this, the subgrid can be ended at the beginning of the lung so that most of the lung is modelled with the main grid. This reduces the computational resources required. A second subgrid is then placed in the middle region of the body, where there are very thin tissues to be modelled, as heart muscle and fat tissue that are thinner than one Δs_a and are modelled with 10 Δs_b, as shown in Fig. 5. After another lung modelled with the main grid, a third subgrid is placed near the end of

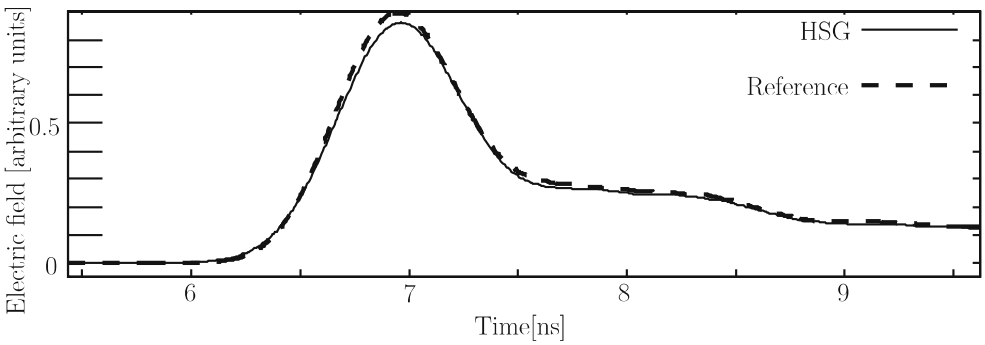

Fig. 6 Electric field at observation point in Fig. 4

the body path to model thin tissues like the skin. Notice that the second and third subgrids are only needed for geometrical reasons, while the first subgrid is needed both for geometrical reasons and for accurate sampling of the high-frequency content of the pulse as it enters the human body. The solid line in Fig. 6 presents the observation. The dotted line in Fig. 6 is the reference signal observed when the entire space is meshed with $\Delta s_{\text{ref}} = \Delta s_b = 2.94/15$ mm. About 3% difference between these two signals is observed in amplitude. The normalised spectrum of these two are almost identical. Computation of 10^5 time steps showed total stability.

4 Conclusions

The modelling of media with high relative permittivity requires a spatial resolution finer than the one imposed by geometrical constraints. Such materials can be modelled efficiently in subgridding schemes. Rigorous derivation of 1D FD HSG–FDTD is performed. The validity of the HSG in the first-order Debye media is examined. The ability of 1D FD HSG–FDTD to handle a high meshing ratio has been exploited in the numerical modelling of a human body. The performance of Huygens surfaces inside the human body has been successfully demonstrated. Moreover, the stability of HSG is better than in a vacuum. No late time instability occurred in all the experiments we performed. The filtering used in [13] is not needed. This is the first step towards 3D modelling.

Future work will target the numerical modelling of the 3D human body using HSG–FDTD. This is a challenging problem because of the complexity of the human body. Ideally, a conformal subgridding would be better to match the complex geometry of the various organs. However, even a rectangular subgridding will permit addressing at least some classes of applications and then very significantly reduce the computational burden in comparisons with calculations with a fine grid in the whole body. As an example, we intend to simulate the propagation of the signal from an electric shock on the surface of the torso for the defibrillation of the ventricles. The optimum location and shape of electrodes, as well as excitation waveform, can be studied through the $\boldsymbol{E}$ field distribution in the heart. The modelling of the heart needs notably high spatial resolution relative to the rest of the torso. This kind of study will benefit significantly from HSG–FDTD by putting only the heart region in the fine mesh.

References

1. Simicevic N (2007) Exposure of biological material to ultra-wideband electomagnetic pulses: dosimetric implications. Health Phys 92:574–583
2. Lin JC (2007) Dosimetric comparison between different quantities for limiting exposure in the RF band: rationale and implications for guidelines. Health Phys 92:547–553
3. Kopecky R, Persson M (2004) Subgridding method for FDTD modeling in the inner ear. Proc SPIE 5445:398–401
4. Zakharian AR, Brio M, Dineen C, Moloney J (2006) Second-order accurate FDTD space and time grid refinement method in three space dimensions. IEEE Photonics Technol Lett 11:1237–1239
5. Donderici B, Teixeira FL (2006) Domain-overriding and digital filtering for 3-D subgridded simulations. IEEE Microw Wirel Compon Lett 16:10–12
6. Kulas L, Mrozowski M (2005) Low-reflection subgridding. IEEE Trans Microwave Theor Tech 53:1587–1592
7. Vaccari A, Pontalti R, Malacarne C, Cristoforetti L (2004) A robust and efficient subgridding algorithm for finite-difference time-domain simulations of Maxwell's equations. J Comput Phys 194:117–139
8. Venkatarayalu NV, Lee R, Gan YB, Li LW (2007) A stable FDTD subgridding method based on finite element formulation with hanging variables. IEEE Trans Antennas Propag 55:907–915
9. Chilton RA, Lee R (2007) Conservative and provably stable FDTD subgridding. IEEE Trans Antennas Propag 55: 2537–2548
10. Marrone M, Mittra R (2005) A new stable hybrid three-dimensional generalized finite difference time domain algorithm for analyzing complex structures. IEEE Trans Antennas Propag 53:1729–1737
11. Xiao K, Pommerenke DJ, Drewniak JL (2007) A three-dimensional FDTD subgridding algorithm with separated temporal and spatial interfaces and related stability analysis. IEEE Trans Antennas Propag 55:1981–1990
12. Kulas L, Mrozowski M (2004) Stability of the FDTD scheme containing macromodels. IEEE Microw Wirel Compon Lett 14:484–486
13. Bérenger JP (2006) A Huygens subgridding for the FDTD method. IEEE Trans Antennas Propag 54:3797–3804
14. Bérenger JP (2005) A FDTD subgridding based on Huygens surfaces. In: IEEE int symp antennas propagat, pp 98–101
15. Huygens C (1690) Treatise on light. http://www.gutenberg.org/etext/14725
16. Taflove A, Hagness SC (2005) Computational electrodynamics. The finite-difference time-domain method. Artech House, Boston, MA
17. Kong JA (1975) Theory of electromagnetic waves. Wiley, New York
18. Debye P (1929) Polar molecules. Dover, New York
19. Gabriel S, Lau R, Gabriel C (1996) The dielectric properties of biological tissues: Iii. parametric models for the dielectric spectrum of tissues. Phys Med Biol 41:2271–2293
20. Costa J, Costen F, Bérenger JP, Brown A (2007) Inclusion of frequency dependency in the Huygens subgridding FDTD for UWB systems. In: IEEE int symp antennas propagat, pp 3077–3080
21. Berenger JP (1994) A perfectly matched layer for the absorption of electromagnetic waves. J Comp Physiol 114:185–200